Multi-Feature Anomaly Detection for Structural Health Monitoring of a Road Bridge using an Autoencoder

Andreas Jansen[1], Karsten Geißler[2]

[1]Department of Steel Structures, Institute of Civil Eng., Technische Universität Berlin, Berlin, Germany
[2]Department of Steel Structures, Institute of Civil Eng., Technische Universität Berlin, Berlin, Germany
email: andreas.jansen@tu-berlin.de, ek-stahlbau@tu-berlin.de

ABSTRACT: Strategies for health monitoring of bridges with new sensors or new signal features are emerging in recent years to overcome the limitations of traditional vibration-based approaches. This paper presents a monitoring system of a road bridge that combines four signal features from different sensor types in order to obtain a holistic picture of the structural condition. These four features are the bearing displacement under temperature load, the natural frequencies and the ratios of integrals (*R-signature*) and extreme values (*M-signature*) of strain and displacement signals during the crossing of vehicles. A derivation of the promising *R-signature* based on influence lines is presented. An anomaly detection approach with an autoencoder is used to identify changes in the patterns of the extracted features that can indicate structural damage as well as faults in the sensing system. The approach is demonstrated with real-world data where an erroneous signal calibration is detected. Signals under structural damage are simulated with a detailed finite element model. It is shown that the anomaly detection procedure can clearly identify the damaged state in the simulated data.

KEY WORDS: SHMII-10; Damage Detection; Anomaly Detection; Autoencoder; Moving Load Response.

1 INTRODUCTION

A key objective for Structural Health Monitoring (SHM) of bridges is the detection of damage at the earliest possible stage. Extensive research exists on the field of vibration-based methods. These methods commonly use accelerometers to monitor the modal characteristics of a structure, i.e. natural frequencies, mode shapes and modal damping. Essential challenges remain in the field: (i) SHM methods are difficult to validate under real-world conditions [1]. Experiments with artificially induced damage to bridges in operation are practically impossible. Only few studies have investigated the effects of artificial damage on bridges with no traffic at the end of their service life, e.g. [2]. Therefore, the effectiveness of damage detection methods is commonly evaluated with simulations or laboratory tests. The complexity of real-world actions on bridges are difficult to account for with these approaches. (ii) Natural frequencies show only small changes as a result to structural damage but (iii) vary due to environmental influences, predominantly temperature [3]. The temperature-dependent stiffness of the asphalt pavement is identified as a main influencing factor [2]. The variations due to external influences can exceed the magnitude of changes caused by structural damage and therefore prevent damage detection.

The dependencies of the vibration response of a structure to external influences can be accounted for by numerical models from the field of *Machine Learning* (ML). These models are based on the data features only, i.e. no physical assumption about the structure is made. Hereby, *feature* is the common term for inputs into a ML-model. Compared to physical models, e.g. *Finite Element* (FE) models, non-physical models tend to be more flexible and commonly less computationally demanding. However, non-physical models can mainly be used to detect the presence of damage. Localisation and assessment of damage requires physical information.

ML-approaches for SHM can roughly be divided into regression models and reconstruction models. Regression models relate an input, e.g. temperature, to an output, e.g. a natural frequency. Depending on the relationship, linear models can be used [4] or non-linear models such as the *Gauss-Process-Regression* (GPR) are required [5]. Other approaches apply the regression to the intermediate steps of a modal analysis procedure such as *Auto Regressive* (AR) models [6].

Reconstruction models replicate the input features considering the substantial patterns of the data. Such models are at the core of many *unsupervised* anomaly detection procedures, e.g. for bank fraud detection or for medical diagnosis (see [7] for a review). The *Principal Component Analysis* (PCA) is a linear reconstruction approach. Applications to vibration-based bridge monitoring can be found already in 2005 [8]. The adaption to non-linear dependencies can be achieved by *piecewise PCA* [9] or *Kernel-PCA* [10]. Autoencoders can be understood as a generalization of the PCA based on neural networks. Early applications to SHM can be found in [11]. More recent publications apply the concept directly to acceleration time-series data, e.g. [12].

Approaches with sensors other than accelerometers and different signal features are pursuit to address the limited sensitivity of modal characteristics to structural damage. The use of inclinometers shows promising results [13] as well as the application of (fibre-optical) strain gauges [14]. The features for strain gauges signals in the later publication include extreme values and integrals during the crossing of vehicles on road bridges.

An anomaly detection scheme for SHM with an autoencoder is presented here (Section 2.1). The presented approach combines four different features from accelerometers, strain

gauges and displacement transducers that are extracted from signals of a road bridge (Section 3). In doing so, a broad picture of the structural condition of the bridge is obtained. A theoretical derivation of a strain gauge signal feature, the *R-Signature*, is given in Section 2.2. The application to real-world data shows that the used autoencoder architecture is suitable to reconstruct the data (Section 4) and to detect faults of the sensing system. To validate that the model can detect structural damage, signals of the bridge in a damaged state are artificially generated with detailed FE-simulations (Section 5 and 6).

2 THEORECTICAL BACKROUND

2.1 Anomaly Detection with Autoencoders

Anomaly detection (e.g. [7]) provides a conceptual framework that can be adapted to bridge SHM. Incoming data is either labelled as *normal*, which refers to an intact condition, or *anomalous*, which indicates the possibility of structural damage or a fault in the monitoring system. The label depends on the reconstruction error of an underlying ML-model. The reconstruction error $\varepsilon(x)$ is calculated as the deviation of new data x compared to the predictions x^* of the model. A vector norm such as the Euclidean distance in Eq. 1 can be used as reconstruction error.

$$\varepsilon(x) = \|x - x^*\|_2 \tag{1}$$

The ML-model is fitted to the data from the structure in an undamaged condition during a *training period*. During application, the condition of the structure is assessed by the reconstruction error. If the bridge undergoes damage, the patterns of the sensor data will change and the model predictions will consequently deviate from the measurements, resulting in a high reconstruction error. The data will be labelled as *anomalous*. Thereafter, the structure as well as the monitoring system must be assessed by experienced engineers to determine the source of the anomaly. Based on this assessment, further steps are initiated.
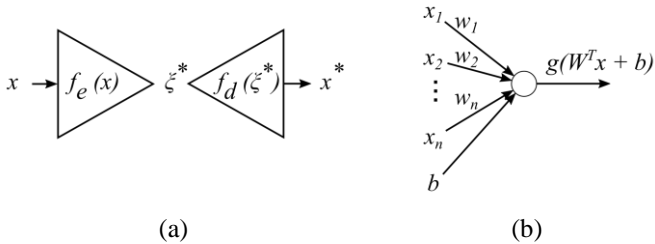

(a)   (b)

Figure 1. (a) Autoencoder (b) Perceptron.

An autoencoder is a type of neural network that can be used for anomaly detection. The basic architecture of an autoencoder consists of two parts (Figure 1a): an encoder $f_e(x)$, which transforms the input data x to a lower dimensional representation ξ^*, and a decoder $f_d(\xi^*)$, which subsequently obtains a reconstruction x^* of the input data . By forcing the data through a lower dimensional bottleneck, also called *code* or *latent representation*, the underlying data structure is captured. A reconstruction approach is different from explicit regression methods for SHM where an input ξ, such as the temperature, is directly mapped to an output x, e.g. natural frequencies, by a model $f(\xi)$. Autoencoders provide the advantage that physical relationships that are unknown or

difficult to measure are implicitly considered through the learnt correlation structure of the data.

Autoencoders can be built with different types of neural networks. Here, the simplest form, a *feed forward Multi-Layer Perceptron* (MLP) network is used. An MLP consist of several layers of stacked perceptrons. Each perceptron calculates the weighted sum $\sum w_j x_j = W^T x$ of its inputs $x^T = [x_1, x_2, \ldots, x_k]$ (Figure 1b) which are the outputs of the previous layer. Hereby, $W^T = [w_1, w_2, \ldots, w_k]$ are the weights. An offset or *bias b* is additionally added to the weighted sum. The possibility to represent non-linear relationships is achieved through a non-linear activation function $g(z = W^T x + b)$. The *rectified linear* function (ReLU) will be used here and is defined as $g(z) = \max\{0, z\}$. The benefit of neural networks with non-linear activation functions and at least one *hidden layer* is that they can approximate almost any function. This is a loose formulation of what is known as the *universal approximation theorem* (details are discussed e.g. in [16]). A hidden layer is one that is not exposed to the input or the output of the neural network.

All autoencoder models in this paper use an architecture with the following five layers: input layer, hidden encoder layer, bottleneck, hidden decoder layer, output layer. The output layer uses a linear activation function. The weights w of the neural network are obtained through optimization with the objective to minimize the mean squared error between input x and output $x^* = (f_d \circ f_e)(x)$ (Eq. 2).

$$\min_w \frac{1}{n} \sum_{i=1}^{n} \left\| x^i - (f_d \circ f_e)_w (x^i) \right\|_2^2 \tag{2}$$

The optimization is conducted with a training data set consisting of n data points. Additionally, 20% of the training data is used for validation. This ensures that the learnt relationship is generally valid and does not hold for the training data only. The Adam-Algorithm (see [16]) is used for minimizing Eq. 2. The data is fed through the network several times during training. Each cycle is called an *epoch*.

2.2 R-Signature

Depending on the architecture, an autoencoder can be used with different types of data, including high dimensional data like images or time series. The presented approach combines four different features that are extracted from the measurement signals (Section 3.2). The approach is non-sequential, i.e. the temporal order of the data is not considered in the model. One of the considered features, the *R-signature*, showed to be significantly more sensitive to structural damage than natural frequencies in the first investigation of the authors [15]. The feature is based on influence lines. A brief derivation shall be given in the following.

The concept of influence lines can be applied to sensors, such that the influence line $\eta_k(x)$ describes the amplitude measured by sensor k as a reaction to a unit load at position x on a beam bridge (Figure 2). The signal measured during the crossing of a vehicle at sensor k shall be defined as $s_k(t)$. Assuming constant vehicle velocity v, the signal can be considered in the space domain as $s_k(x) = s(t \cdot v)$. If the static structural response is linear, $s_k(x)$ can be calculated according to Eq. 3 as the superposition of the reactions to N axle loads P_i, where

x describes the position of the first axle and a_i is the distance of axle i to the first axle. These considerations hold for all sensors that measure displacement related properties, e.g. strain gauges, displacement transducers or inclinometers.
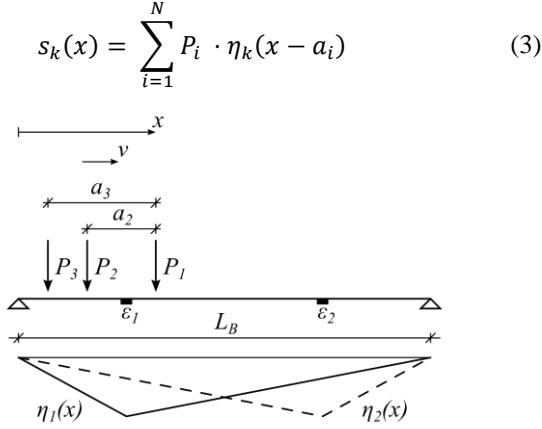
$$s_k(x) = \sum_{i=1}^{N} P_i \cdot \eta_k(x - a_i) \qquad (3)$$

Figure 2. Schematic illustration of the crossing of a vehicle on a single span beam bridge

It can be shown that the integral I_k over $s_k(x)$ is proportional to the gross vehicle weight (Eq. 4). For this purpose, the integration limits are chosen to be $x = 0$ and $x = L_B + L_V$, where L_B is the length of the bridge and $L_V = a_N$ is the length of the vehicle. The integral can be expressed as the sum of the integrals over the signal contributions of every axle i. The influence line $\eta(x)$ only has values $\neq 0$ in the interval $[0, L_B]$. Therefore, $\int_0^{L_B+L_V} \eta_k(x - a_i)dx$ simplifies to $\int_0^{L_B} \eta_k(x)dx$. As a result, I_k is reduced to the product between the gross vehicle weight $\sum P_i$ and the integral over the influence line of the considered sensor.

$$
\begin{aligned}
I_k &= \int_0^{L_B+L_V} s_k(x)dx \\
&= \int_0^{L_B+L_V} \sum_{i=1}^{N} P_i \cdot \eta_k(x - a_i)dx \\
&= \sum_{i=1}^{N} \left(P_i \int_0^{L_B+L_V} \eta_k(x - a_i)dx \right) \\
&= \sum_{i=1}^{N} P_i \cdot \int_0^{L_B} \eta_k(x)dx
\end{aligned}
\qquad (4)
$$

The relationship from Eq. 4 can be used for bridge weight in motion systems. Here, it will be used to create a feature that is independent of vehicle weight and axle distances. The feature considers the ratio of the integrals I_j and I_k over the signals from the sensors j and k (Eq. 5). It shall be referred to as *R-value*. It can be seen from Eq. 5 that the vehicle weight cancels out. Because $s_j(x)$ and $s_k(x)$ undergo the same transformation to the space domain, the ratio can also be calculated in the time domain. For this case, the upper integration limit is the duration T of the vehicle crossing. Within classical beam theory the R-value is constant.

It applies that $R(s_j, s_k) = R(s_k, s_j)^{-1}$. Therefore, there are $n(n-1)/2$ distinct R-values. The vector of all R-values shall be referred to as *R-signature*. Like a vibration mode shape, the R-signature provides information about the stiffness distribution over the structure. Severe structural damage changes the stiffness distribution and leads e.g. to an increase in the amplitudes of some sensor signals while the signals from sensors which are further away from the damage location remain relatively unaffected. This results in a deviation of the R-signature which can be used to identify the presence of the damage. It shall be noted that there are cases possible where the influence lines of several sensors change in a similar fashion due to damage. However, it is assumed that the risk of an undetectable severe damage case is relatively low with multiple spatially distributed sensors in longitudinal and transversal direction. The R-signature can be used as a feature for damage detection with physical (e.g. FE-Update) as well as non-physical models (e.g. ML).

$$
\begin{aligned}
R(s_j, s_k) &= \frac{I_j}{I_k} = \frac{\sum_{i=1}^{N} P_i \cdot \int_0^{L_B} \eta_j(x)dx}{\sum_{i=1}^{N} P_i \cdot \int_0^{L_B} \eta_k(x)dx} \\
&= \frac{\int_0^{L_B} \eta_j(x)dx}{\int_0^{L_B} \eta_k(x)dx} \\
&= \frac{\int_0^{T} s_j(t)dt}{\int_0^{T} s_k(t)dt} = const.
\end{aligned}
\qquad (5)
$$

Following limitations apply to the use of the R-signature: (i) Only the quasi-static response is considered. Hence, if the sensor signals contain significant amplitudes from dynamic structural response, the calculation of the R-signature can be flawed. (ii) In order to calculate the R-Signature, the crossings of single vehicles need to be isolated in the measurement data. This might not be feasible for large bridges.

The concept of the R-signature is derived from one dimensional beam theory. However, the position of a vehicle in transversal direction on a lane varies on a real bridge. The influence of the transversal vehicle position on the R-signature is investigated in [15] using the same bridge as here as an example. Simulations show that the influence of transversal vehicle position on the R-values is approximately linear within a lane. Therefore, an anomaly detection procedure with the linear PCA is applied. The procedure is validated for damage detection with the simulated data. It is shown that the PCA-procedure can also be applied to real-world data with a limited selection of strain gauges. However, when also considering the signals from displacement transducers at the roller bearing for the R-values, the dependencies become non-linear due to effects such as temperature and friction. The PCA is insufficient to account for these effects. To address these shortcomings, the presented approach with an autoencoder is applied.

3 EXAMPLE BRIDGE

3.1 Sensor Layout

The anomaly detection approach shall be demonstrated on a hollow section girder steel road bridge. The single span bridge (L = 47 m) from 1971 is horizontally curved (R = 525 m) and oblique-angled (Figure 3). A heavily frequented federal road runs over the bridge on separate superstructures for each direction. Due to corrosion damage, traffic is limited to one lane per direction.
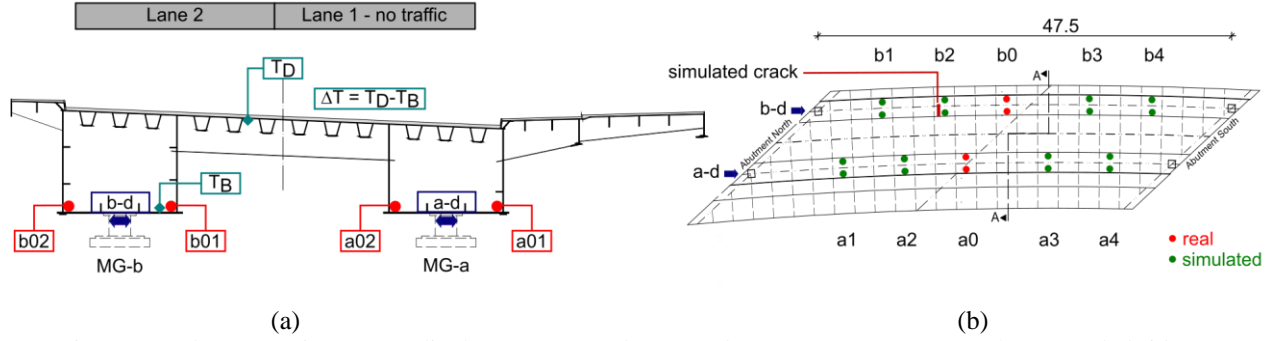
(a) (b)

Figure 3. Relevant strain gauges, displacement transducers and temperature sensors on the example bridge: (a) cross section (b) plan view.

A sensor system consisting of accelerometers, displacement transducers, strain gauges and temperature sensors is used to continuously monitor the structural health of the bridge. Only the data of one of the superstructures is discussed in the following. The displacement of the roller bearings is measured with one displacement transducer for each bearing (a-d, b-d, Figure 3). Two accelerometers are placed at mid-span to obtain the vibration characteristics of the bridge. Four strain gauges are placed at mid-span on the webs close to the bottom chord of the respective main girders.

Due to the oblique-angled layout, the strain gauges at girder a (a01, a02) and b (b01, b02) do not lie between the same cross members. The open traffic lane is above main girder MG-b. Additional strain gauges for a bridge weigh-in-motion system are located on the ribs of the bridge deck and the cross members. However, these sensors will not be considered for health monitoring.

The temperature of the bridge, as well as the outside temperature, is measured with a total of 10 temperature sensors. The evaluation showed that the temperature below the bridge deck T_D and at the bottom chord of the main girder T_B have the largest influence. Temperature sensors are sampled with 1 Hz and all other sensors with 50 Hz.

The signals of the strain gauges and the displacement transducer can be partitioned according to the primary load acting on the bridge during the considered time instance. For smaller road bridges the main loads are traffic and temperature. Effects due to wind load are mostly insignificant. The signals could further be divided into *dynamic* and *quasi-static* components according to their frequency content. Here, components with frequencies close to or above the first natural frequency of the system can be defined as dynamic. Components with frequencies below the first natural frequency can be described as quasi-static. Additionally, the signals can contain errors such as electrical noise, hum or sensor drifts.

3.2 Feature Extraction

In a pre-processing step, a segmentation according to the primary load (traffic or temperature) on the bridge is performed. A further decomposition through frequency filters showed no clear benefit. Features are subsequently calculated separately for segments x_V during which vehicles cross the bridge and segments x_T that contain mainly effects due to temperature load. Time windows for x_V are zeroed according to the preceding values of x_T. The following features are extracted:

R-signature: The numerical integral I over x_V is calculated for the strain gauges (a01, a02, b01, b02) and the two displacements transducers at the roller bearings (a-d, b-d) for each vehicle crossing (Figure 4). All combinations of R-values are then calculated with Eq. 5, resulting in a 15-dimensional feature vector.

M-signature: Additionally to the numerical integral, the extreme value E of x_V is also calculated for every vehicle crossing (Figure 4). Similar to the R-values, the ratios between different sensors are obtained according to Eq. 6. Although a theoretical relationship has not yet been derived, it can be observed (Section 4) that the values show correlations which can be useful in detecting anomalies. The M-values are calculated for the same sensors as the R-values, which leads to another 15-dimensional feature vector.

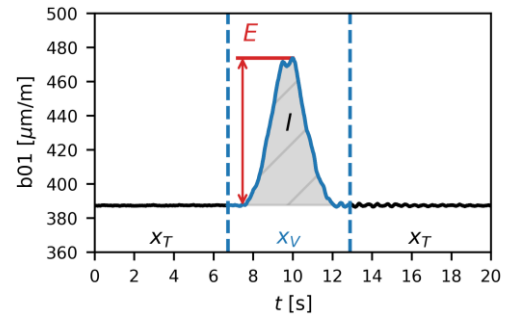$$M(s_j, s_k) = \frac{E_j}{E_k} = \frac{\max\{|s_j(t)|\}}{\max\{|s_k(t)|\}} \tag{6}$$

Figure 4. Illustration of the feature extraction

Temperature-dependent Displacement: The 15-min average of the signal part x_T is obtained for the displacement transducers (a-d, b-d) as another feature. This feature is useful to monitor the temperature-dependent displacement of the roller bearings.

Natural Frequencies: The *Frequency Domain Decomposition* (FDD) is used to calculate natural frequencies and mode shapes from 15-min time windows of the accelerometer signals. The first two natural frequencies with an average of $\bar{f}_1 = 2.19\ Hz$ and $\bar{f}_2 = 3.37\ Hz$ can be identified reliably and are therefore considered as features. It has been investigated if more variance of the natural frequencies can be explained by using only the free decay response after the crossing of vehicles for modal analysis. However, no clear dependency of the natural frequencies and factors, such as the

maximum strain or acceleration amplitude, could be determined. Because the number of vehicle crossings with an undisturbed free decay response is limited, modal analysis is carried out without distinguishing between the signal parts x_V or x_T.

Lastly, the temperatures at the deck (T_D) and the bottom chord (T_B) are also used for the autoencoder which leads to a total of 36 features for each isolated crossing of a vehicle. Features that are independent of vehicle crossings are taken from the respective 15-min time window in which the crossing falls.

4 APPLICATION TO REAL-WORLD DATA

The anomaly detection procedure is demonstrated with real-world data between July 2019 and May 2020. The data until March 2020 is used for the training of the autoencoder of which 80% is used for the actual learning and 20% serves for validation. The application of the autoencoder is demonstrated with the data from March and April 2020. On the 9th of April, a restart of the monitoring system led to an erroneous calibration of the signals from the displacement transducers. This error remains in the application data to show the ability of the presented approach to detect faults of the sensing system.

Vehicles with a gross weight approximately between 16 t and 60 t are used for anomaly detection. During weekdays an average of 125 vehicles fall into this category. On Saturdays the average is 25 vehicles and on Sundays it is only 10. The lower number on weekends leads to less reliable predictions. This issue is addressed by a variable error threshold in [15]. For simplicity, a constant threshold is used here.

Figure 5 shows the pairwise dependencies of some of the features. The R- and M-values between the strain gauges show linear dependencies between each other. No clear dependency between the R-/M-values and temperature is visible. R-values that consider the bearing displacements (e.g. b-d) show a non-linear relationship with other R-values as well as with temperature or the natural frequencies. The temperature-dependent bearing displacement has a clear linear correlation with T_D. The natural frequencies show non-linear behaviour with respect to temperature and thus with respect to the bearing displacements as well. An increase of frequency, i.e. a stiffening of the structure, is visible for high as well as for low temperatures.

It is known from other publications (e.g. [2]) that the asphalt layer has a contribution to the stiffness of a bridge and that the asphalt stiffness changes in a non-linear fashion with respect to temperature. However, it becomes clear from Figure 5 that temperature is not the only source for non-linearity for the features $R(b\text{-}d, b01)$ and f_2 as large proportions of the variance remains unexplained. It is assumed that the friction in the roller bearings are another significant source for non-linear behaviour. The specific relationships have not yet been clarified.
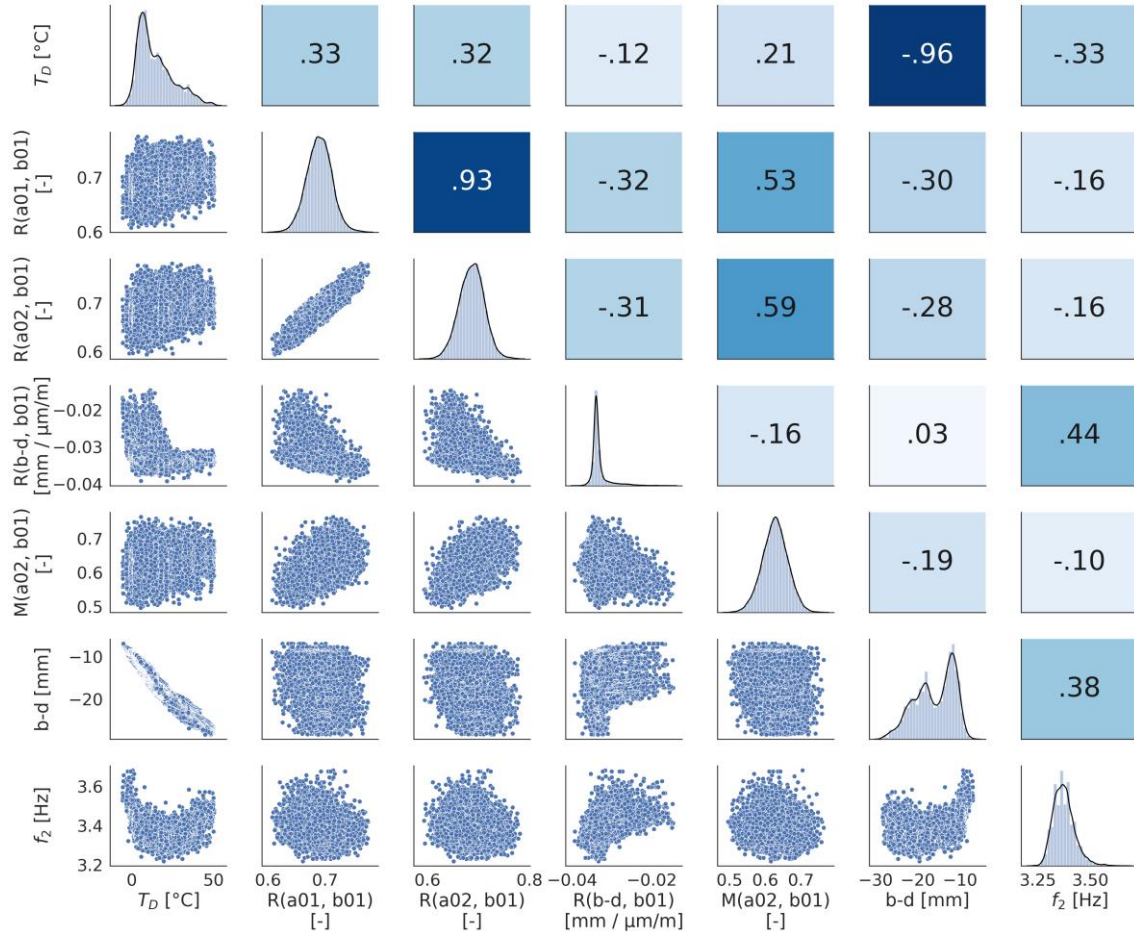
Figure 5. Correlation structure of selected features of the real-world data. Lower triangular matrix: scatter plot, diagonal: density distribution, upper triangular matrix: Pearson's correlation coefficient

The application of the autoencoder provides the benefit that dependencies from influences that are unclear or not measurable can be implicitly captured. In the comparison of several configurations, an autoencoder with a hidden layer size of 60 neurons and a bottleneck layer size of 18 neurons showed the best result. A lower size of the bottleneck layer does not result in a consistent reconstruction error over the training period. Increasing the size of the latent space can lead to the learning of an identity function and might therefore be useless for anomaly detection. A compression rate of $18/36 = 0.5$ appears to be a suitable compromise.

The features are standardised to zero mean and unit variance before being fed to the model. The application data is also standardised by the mean and variance of the training data. The network is trained for 300 epochs. No significant model improvement can be noticed towards the end of the training. The training and test accuracy are approximately equal around 0.97 where an accuracy of 1.0 indicates perfect reconstruction.

Euclidean distance (Eq. 1) is used as the reconstruction error in standardised coordinates. In most cases, structural damage or faults of the sensing system would manifest themselves permanently. Based on this assumption, anomaly detection is conducted with the daily median of the reconstruction error. In doing so, the influence of anomalies of single crossings that arise, e.g. from errors in the pre-processing, are weakened. A log-normal distribution is fitted to the daily median and an error threshold is chosen as the 99th-percentile (Figure 6). The resulting threshold value is 0.082. Few anomalies can be seen during the training period in Figure 7a. Under the assumption that the structure is undamaged during this period these anomalies are *false positive*. It is interesting that the false positive anomalies arise on the coldest days of the measurement period (2019-11-30, 2020-01-02) with temperatures between -3 °C and -5 °C. This indicates that the autoencoder does not reflect the data sufficiently under these rare conditions. More training data under extreme temperatures would be needed to achieve a better model fit.

The incoming data is clearly identified as anomalous after the 9th of April, as the median of the reconstruction error increases to values above 0.7 (Figure 7b). If the reconstruction error exceeds the threshold permanently, a thorough investigation into the source of an anomaly is mandatory. This investigation can be challenging as it requires interdisciplinary knowledge in the areas of machine learning, electrical and structural engineering. In the presented case, the source of the anomaly

could be identified as the erroneous offset in the signals of the displacement transducers. The detection of the signal offset demonstrates that the autoencoder is suitable to identify changes in the data structure due to faults in the sensing system and likely also due to structural damage.
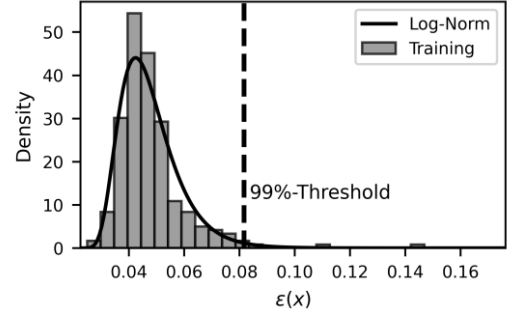

Figure 6. Reconstruction error of the real-world training data with a log-normal distribution

5 SIMULATION

Detailed FE-simulations are conducted to evaluate if the procedure is also able to detect structural damage. Sensor signals are simulated in a damage state of the bridge under realistic operational loads. The assumed damage condition is a severe fatigue crack in the main girder *b*. The crack lies at the location of a change in thickness of the bottom chord at around a third of the girder length (Figure 3). Four damaged scenarios S1 to S4 with increasing crack length are distinguished. The undamaged condition is referred to as S0. In scenario S1 the crack starts from the inner side of the girder with a length of 20 cm (S2: 40 cm, S3: 80 cm). Scenario S4 assumes the brittle fracture of the entire bottom chord. Modelling of the crack is achieved by decoupling the edges of the shell elements in the FE-model. All FE-calculation are based on linear-elastic material behaviour. Therefore, non-linear effects such as local yielding in the crack area are not taken into account.

The FE-model (Figure 8) is used to calculate grid points for interpolation surrogate models using cubic spline interpolation [17]. The simulations are subsequently conducted with the interpolation models. Different surrogate models are created for each damage scenario. The input data for the simulations is described in the following:
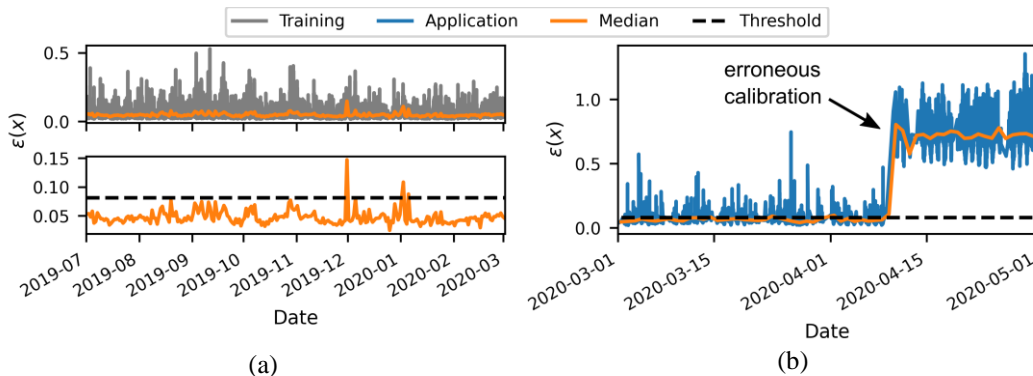

(a)   (b)

Figure 7. Anomaly detection with real-world data: (a) training period (b) application period

Asphalt Stiffness: An asphalt layer on the bridge deck is included in the FE-model. A non-linear temperature-dependent stiffness is considered. The asphalt temperature is assumed to be equal to the temperature at sensor T_D. The temperature-dependent asphalt stiffness is the only parameter used for the interpolation model for the natural frequencies. A grid of eight values between -20 °C and 50 °C is used.
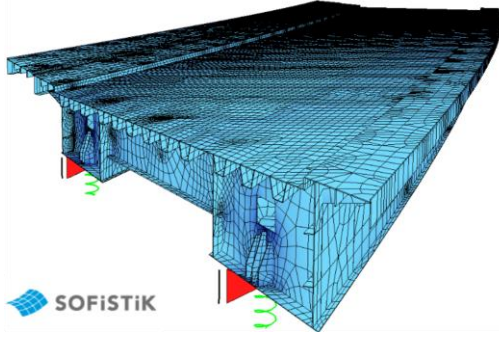

Figure 8. Detailed FE-model of the example bridge

Temperature Load: The input data for the temperature load is directly adopted from the real measurement data. A constant temperature load is applied to all elements of the bridge deck according to the measurement values of sensor T_D. Analogously, a constant temperature is applied to the bottom chords according to sensor T_B. A linear vertical gradient is assumed in the webs. The response to temperature load is calculated for the strain gauges and displacement transducers. Eight grid points are used for the deck temperature T_D. Additionally, 12 grid points are considered for T_B for every T_D to account for variations of the vertical temperature gradient.

Traffic Load: The data for the axle loads and the vehicle geometry is taken from a weigh-in-motion station and was kindly provided by the German Federal Highway Research Institute (BASt). The velocity of the vehicles is assumed to be normally distributed with a mean value of 30 km/h and a standard deviation of 5 km/h. As is the case on the real bridge, traffic is only considered on lane 2. The position of the vehicles in transversal direction is assumed to be normally distributed with a standard deviation σ of 17 cm. The expected value corresponds to the centre of the lane. The range of values is approximately $\pm 3\sigma = 0.5$ m. The crossing of a vehicle is simulated for every 30 minutes resulting in 48 crossings per day. Only vehicles above a gross vehicle weight of 7.5 t are considered. Daily and weekly variations of traffic characteristics are taken into account in the simulation, i.e. the data is divided in 3-hour windows and between weekdays, Saturdays and Sundays. For example, a vehicle sample for Sunday at 04:30 is drawn from data from Sundays between 03:00 and 06:00.

The static structural response to the crossing of a vehicle is calculated by independently obtaining the response for each axle and subsequently superimposing the results. This approach corresponds to Eq. 3, however, the influence line is an interpolation model $\eta(x, y, T_D)$ that considers the longitudinal axle position x, the transversal axle position y, and the temperature of the asphalt layer T_D. Grid points are obtained with an axle load of 100 kN in 63 axle positions along the longitudinal direction and five in transversal direction. Again,

eight temperature grid points are considered, resulting in 2520 FE-solutions per damage scenario.

Feature extraction is carried out in a similar fashion as for the real-world data, resulting in the same 36 features. The simulated R-/M-values of the strain signals also show a linear relationship between each other (see Figure 9). The values and the variance are comparable to the real-world data. R-values that contain the displacement of the bearings as well as the natural frequencies show non-linear dependencies with temperature and other features. The variance of e.g. *R(b-d, b01)* or f_2 is significantly lower than in the real-world data. This indicates that not all influences are accounted for in the simulation.

6   DAMAGE DETECTION WITH SIMULATED DATA

The training period in the undamaged scenario S0 is chosen between July 2019 and the 21st of February 2020. Thereafter, two weeks are simulated for each scenario as application data.

The same autoencoder architecture is used for the simulation as for the real-world data. Although a lower compression rate than 0.5 is feasible to achieve high model accuracy with the simulated data, it is crucial to investigate if damage detection can be achieved with the chosen compression rate. Therefore, 18 neurons are used in the bottleneck layer.

The results of the anomaly detection procedure are illustrated in Figure 10. The 99th-percentile threshold of the log-normal distribution fitted to the daily median of the reconstruction error is 0.029. There are some anomalies in the training period, also on days with very low temperatures. As can be seen, the error threshold is clearly exceeded in the damage scenarios S1-S4. The *true positive* rate is 100%. Median errors up to 24.5 are observed in S1-S3 which is more than 800 times the threshold. An interesting observation is that the reconstruction error does not increase with progressing damage severity. No difference in the magnitude of the reconstruction error is noticeable for the scenarios S1-S3.

In further investigations, it is assessed if damage detection with an autoencoder and a compression rate of 0.5 is also possible using the extreme values and integrals directly as features, i.e. without calculating the signatures beforehand. Although damage can be identified, the reconstruction error is significantly less sensitive. Therefore, a calculation of the R-/M-signatures in the pre-processing step is preferred. Based on the simulation, the conclusion is drawn that a similar damage case can be identified with a high probability in the real-world data using the presented approach with the R-/M-signature.

7   CONCLUSION

The findings of this article can be summarized as follows:
- The measurement signals can be segmented into intervals with traffic load and intervals with predominantly temperature load. Four different features are extracted: the R- and M-signature for crossing vehicles, the displacement of the bearings under temperature load, and natural frequencies. In total, a 36-dimensional feature vector is obtained for every vehicle crossing. A theoretical derivation of the R-signature based on influence lines is given.
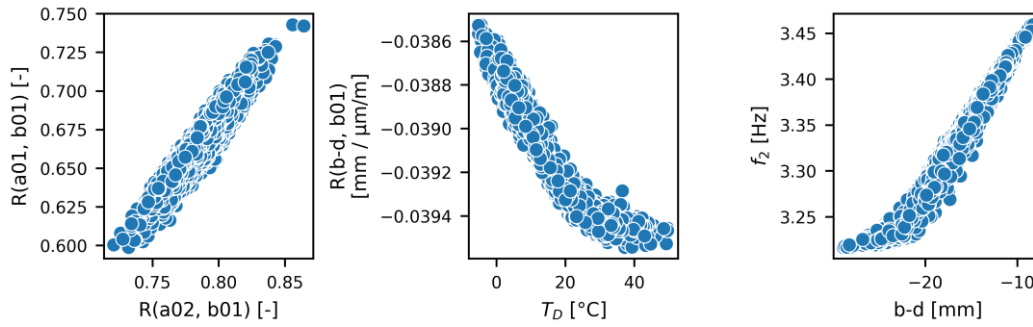
Figure 9. Correlation structure of selected features of the simulated data
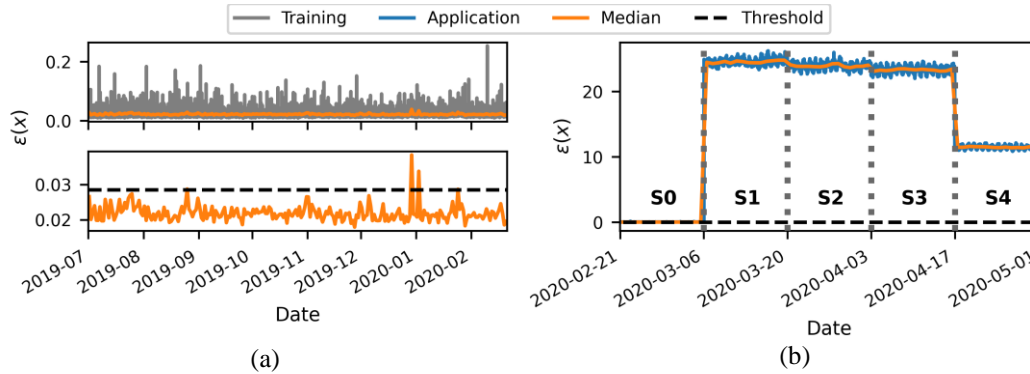

(a)

(b)

Figure 10. Anomaly detection with simulated data: (a) training period (b) application period

- An autoencoder with five perceptron layers is suitable to reconstruct the non-linear real-world monitoring data. A compression rate of 0.5 is required to achieve a high accuracy of the model. It is observed that the anomaly detection procedure can detect the erroneous offset of sensor signals.

- A crack in the bottom chord is simulated with an FE-model of the bridge under realistic temperature and traffic loads. The simulated data shows similar non-linear dependencies as the real-world data. In order to investigate if the procedure can also detect structural damage, an autoencoder with the same architecture and compression rate as for the real-world data is used with the simulation. Damage is clearly identified.

- The simulation shows that the reconstruction error does not necessarily increase with progressing damage severity. Moreover, the procedure gives no insights into the sources of anomalies. Further research is required on methods to simplify the interpretation of anomalies. A combination or a coupling of different types of models, physical and non-physical, could be effective for this task.

ACKNOWLEDGEMENTS

REFERENCES

[1] J.M. Brownjohn, et al., *Vibration-based monitoring of civil infrastructure: challenges and successes*, Journal of Civil Structural Health Monitoring, 1(3-4), 79-95, 2011.

[2] B. Peeters and G. De Roeck, *One-year monitoring of the Z24-Bridge: environmental effects versus damage events*, Earthquake Engineering & Structural Dynamics, 30(2), 149-171, 2001.

[3] W. Fan and P. Qiao, *Vibration-based damage identification methods: a review and comparative study*, Structural Health Monitoring, 10(1), 83-111, 2011.

[4] N. Dervilis, et al., *On robust regression analysis as a means of exploring environmental and operational conditions for SHM data*, Journal of Sound and Vibration, 347, 279-296, 2015.

[5] K. Worden and E.J. Cross, *On switching response surface models, with applications to the structural health monitoring of bridges,* Mechanical Systems and Signal Processing, 98, 139-156, 2018.

[6] L. D. Avendaño-Valencia, et al., *Gaussian process time-series models for structures under operational variability*, Frontiers in Built Environment, 3, 69, 2017.

[7] L. Ruff, et al., *A Unifying Review of Deep and Shallow Anomaly Detection* arXiv preprint arXiv:2009.11732, 2020.

[8] A.M. Yan, et al., *Structural damage diagnosis under varying environmental conditions—part I: a linear analysis*. Mechanical Systems and Signal Processing, 19(4), 847-864, 2005.

[9] A.M. Yan, et al., *Structural damage diagnosis under varying environmental conditions—part II: local PCA for non-linear cases*, Mechanical Systems and Signal Processing, 19(4), 865-880, 2005.

[10] A. Deraemaeker, et al., *Vibration-based structural health monitoring using output-only measurements under changing environment*, Mechanical Systems and Signal Processing, 22(1), 34-56, 2008.

[11] E. Figueiredo, et al., *Machine learning algorithms for damage detection under operational and environmental variability*, Structural Health Monitoring, 10(6), 559-572, 2011.

[12] X. Ma, et al., *Structural damage identification based on unsupervised feature-extraction via Variational Auto-encoder*. Measurement, 107811, 2020.

[13] F. Huseynov, et al., *Bridge damage detection using rotation measurements–Experimental validation*, Mechanical Systems and Signal Processing, 135, 106380, 2020.

[14] S Z. Chen, et al., *Comparative study of damage detection methods based on long-gauge FBG for highway bridges*, Sensors, 20(13), 3623, 2020.

[15] A. Jansen and K. Geißler, *Strukturüberwachung von Straßenbrücken durch Bauwerksmonitoring mit einem auf Einflusslinien basierenden Merkmal*, Der Bauingenieur (in press).

[16] I. Goodfellow, et al., *Deep learning,* MIT press, Cambridge, USA, 2016.

[17] T. Böhl, *Master's Thesis: Simulation von Messdaten einer Straßenbrücke mit Schäden unter realitätsnaher Verkehrs- und Temperatureinwirkung*, Supervisors: A. Jansen and K. Geißler, TU Berlin, (in preparation).